THz porous fibers: design, fabrication and experimental characterization

Shaghik Atakaramians[1,2], Shahraam Afshar V.[1], Heike Ebendorff-Heidepriem[1], Michael Nagel[3], Bernd M. Fischer[2], Derek Abbott[2] and Tanya M. Monro[1]

[1]*Centre of Expertise in Photonics, School of Chemistry & Physics, The University of Adelaide, SA 5005 Australia*
[2]*Centre for Biomedical Engineering, School of Electrical & Electronic Engineering, The University of Adelaide, SA 5005 Australia*
[3]*Institut für Halbleitertechnik, RWTH Aachen University Sommerfeldstr. 24, 52074 Aachen*
shaghik@eleceng.adelaide.edu.au

Abstract: Porous fibers have been identified as a means of achieving low losses, low dispersion and high birefringence among THz polymer fibers. By exploiting optical fiber fabrication techniques, two types of THz polymer porous fibers—spider-web and rectangular porous fibers— with 57% and 65% porosity have been fabricated. The effective refractive index measured by terahertz time domain spectroscopy shows a good agreement between the theoretical and experimental results indicating a lower dispersion for THz porous fiber compared to THz microwires. A birefringence of 0.012 at 0.65 THz is also reported for rectangular porous fiber.

OCIS codes: (260.3090) Infrared, far; (060.2280) Fiber design and fabrication; (230.7370) Waveguides; (260.2030) Dispersion; (260.1440) Birefringence.

References and links

1. S. Atakaramians, S. Afshar Vahid, B. M. Fischer, D. Abbott, and T. M. Monro, "Porous fibers: a novel approach to low loss THz waveguides," Opt. Express **16**, 8845–8854 (2008).
2. L.-J. Chen, H.-W. Chen, T.-F. Kao, J.-Y. Lu, and C.-K. Sun, "Low-loss subwavelength plastic fiber for terahertz waveguiding," Opt. Lett. **31**, 308–310 (2006).
3. S. Afshar Vahid, S. Atakaramians, B. M. Fischer, H. Ebendorff-Heidepriem, T. M. Monro, and D. Abbott, "Low loss, low dispersion T-ray transmission in microwires," in *CLEO/QELS*, p. JWA105 (Baltimore, Maryland, 2007).
4. W. Withayachumnankul, G. M. Png, X. Yin, S. Atakaramians, I. Jones, H. Lin, B. Ung, J. Balakrishnan, B. W.-H. Ng, B. Ferguson, S. P. Mickan, B. M. Fischer, and D. Abbott, "T-ray sensing and imaging," Proc. IEEE **95**, 1528–1558 (2007).
5. J.-Y. Lu, C.-P. Yu, H.-C. Chang, H.-W. Chen, Y.-T. Li, C.-L. Pan, and C.-K. Sun, "Terahertz air-core microstructure fiber," Appl. Phys. Lett. **92**, 064105 (2008).
6. K. Nielsen, H. K. Rasmussen, A. J. L. Adam, P. C. M. Planken, O. Bang, and P. U. Jepsen, "Bendable, low-loss Topas fibers for the terahertz frequency range," Opt. Express **17**, 8592–8601 (2009).
7. B. Bowden, J. A. Harrington, and O. Mitrofanov, "Silver/polystyrene-coated hollow glass waveguides for the transmission of terahertz radiation," Opt. Lett. **32**, 2945–2947 (2007).
8. A. Hassani, A. Dupuis, and M. Skorobogatiy, "Porous polymer fibers for low-loss Terahertz guiding," Opt. Express **16**, 6340–6351 (2008).
9. A. Hassani, A. Dupuis, and M. Skorobogatiy, "Low loss porous terahertz fibers containing multiple subwavelength holes," Appl. Phys. Lett. **92**, 071101 (2008).
10. S. Atakaramians, S. Afshar, B. M. Fischer, D. Abbott, and T. M. Monro, "Low loss, low dispersion and highly birefringent terahertz porous fibers," Opt. Commun. **282**, 36–38 (2008).
11. H. Han, H. Park, M. Cho, and J. Kim, "Terahertz pulse propagation in a plastic photonic crystal fiber," Appl. Phys. Lett. **80**, 2634–2636 (2002).

#111989 - $15.00 USD Received 1 Jun 2009; revised 24 Jul 2009; accepted 24 Jul 2009; published 29 Jul 2009

12. M. Cho, J. Kim, H. Park, Y. Han, K. Moon, E. Jung, and H. Han, "Highly birefringent terahertz polarization maintaining plastic photonic crystal fibers," Opt. Express **16**, 7–12 (2008).
13. C. S. Ponseca, R. Pobre, E. Estacio, N. Sarukura, A. Argyros, M. C. J. Large, and M. A. van Eijkelenborg, "Transmission of terahertz radiation using a microstructured polymer optical fiber," Opt. Lett. **33**, 902–904 (2008).
14. T. M. Monro and H. Ebendorff-Heidepriem, "Progress in microstructured optical fibers," Annual Review of Materials Research **36**, 467–495 (2006).
15. A. Dupuis, J.-F. Allard, D. Morris, K. Stoeffler, C. Dubois and M. Skorobogatiy, "Fabrication and THz loss measurements of porous subwavelength fibers using a directional coupler method," Opt. Express **17**, 8012–8028 (2009).
16. G. Barton, M. A. van Eijkelenborg, G. Henry, M. C. J. Large, and J. Zagari, "Fabrication of microstructured polymer optical fibres," Optical Fiber Technology **10**, 325–335 (2004).
17. H. Ebendorff-Heidepriem and T. M. Monro, "Extrusion of complex preforms for microstructured optical fibers," Opt. Express **15**, 15,086–15,096 (2007).
18. H. Ebendorff-Heidepriem, T. M. Monro, M. A. van Eijkelenborg, and M. C. J. Large, "Extruded high-NA microstructured polymer optical fibre," Opt. Commun. **273**, 133–137 (2007).
19. S. H. Law, M. A. van Eijkelenborg, G. W. Barton, C. Yan, R. Lwin, and J. Gan, "Cleaved end-face quality of microstructured polymer optical fibres," Opt. Commun. **265**, 513–520 (2006).
20. M. Wächter, M. Nagel, and H. Kurz, "Metallic slit waveguide for dispersion-free low-loss terahertz signal transmission," Appl. Phys. Lett. **90**, 061111 (2007).
21. D. Grischkowsky, "Optoelectronic Characterization of Transmission Lines and Waveguides by Terahertz Time-Domain Spectroscopy," IEEE Journal on Selected Topics in Quantum Electronics **6**, 1122–1135 (2000).
22. S. Atakaramians, S. Afshar Vahid, B. M. Fischer, H. Ebendorff-Heidepriem, T. M. Monro, and D. Abbott, "Low loss terahertz transmission," in *Proceedings SPIE Micro- and Nanotechnology: Smart Materials, Nano- and Micro-Smart Systems*, vol. 6414 (art. no. 64140I, Adelaide, Australia, 10-13 Dec., 2006).

1. Introduction

In recent years there has been increased interest in low loss and low dispersion THz waveguides as potential substitutes for free-space optics in terahertz spectroscopy and imaging systems that require greater electromagnetic confinement. A number of waveguide solutions based on technologies from both microwave and optics, as reviewed in Ref [1], have been studied. Among the dielectric solutions proposed, solid-core sub-wavelength fibers [2] (so-called THz microwires [3, 4]), hollow-core and solid-core microstructured fibers [5, 6], and Ag/PS-coated hollow-core glass fibers [7] have the lowest loss reported in the literature. These waveguide solutions are either large in diameter (20-30 mm), which reduces the flexibility of the waveguide structure, or are only suitable for relatively narrow band applications due to limitation in photonic bandgap bandwidth or loss restrictions.

Recently, a novel class of THz fibers, porous fibers, was proposed [1, 8, 9]. These fibers are air-clad fibers with diameters less than or comparable to the operating wavelengths ($\leq 600\ \mu$m) with sub-wavelength features in the core, which allow low loss propagation and improved confinement of the field compared to microwires [1]. It is also theoretically demonstrated [10] that porous fibers have a smaller decrease in the group velocity, i.e. lower dispersion, relative to microwires. Furthermore it has been shown [10] that these fibers can be designed to maintain polarization of the field by using asymmetrical sub-wavelength air-holes.

In terms of state of the art in THz waveguide fabrication, THz hollow-core and solid-core microstructured fibers [5, 11, 12] have been fabricated by stacking teflon or high density polyethylene capillary tubes. The tubes were stacked to form a two dimensional triangular lattice and then were fused together by either using thin layers of polyethylene film or by heat treatment. No fiber drawing was required for these THz waveguides since the dimension achieved by stacking was suited for THz guidance. Another approach proposed for fabrication of a THz solid- and hollow-core microstructured polymer waveguides [6, 13] was drilling the hole pattern into a 60-70 mm diameter of polymer preform using a computer controlled mill, and drawing the preform down to 6 mm diameter fiber.

Porous fibers have outer diameters less or comparable to the operating wavelength

#111989 - $15.00 USD Received 1 Jun 2009; revised 24 Jul 2009; accepted 24 Jul 2009; published 29 Jul 2009

($\leq$ 600 μm), resulting in sub-wavelength features within the transverse profile of the fibers. For preforms produced using the stacking method, the stacked preform needs to be drawn. As is known from optical fiber fabrication, to accomplish that, the bundle is usually held together by an outer jacket [14] to enable pressurization of the holes in the preform. The hole closure possibility is very high in this method and the maximum achieved porosity so far is 8-18% [15]. Moreover this method is suitable for fabrication of porous fiber with hexagonal array of circular air-holes. The fabrication of a fiber made by drilling the holes in the preform is very time consuming for a large number of holes and this method has restricted maximum porosity due to the mechanical constraints of the hole size and the wall thickness between the holes [16]. Furthermore the shape of the holes is limited to the circular shape.

Dupuis et al. have proposed a subtraction technique for porous fiber fabrication [15]. In this method after drawing down the composite preform, the fiber segments were submerged into a solvent for several days to etch away the material residing in holes. The fibers were also left to dry for several days. Although the air-holes were preserved in this method, the fabrication process in very lengthy and the choice of material is limited in terms of dissolving solvent and melting temperature differences between the materials. Large melting temperature differences can result in material degradation. Moreover the maximum porosity achieved was 29-45%.

In terms of loss values characterization of porous fibers, recently, Dupuis et al. have reported loss values of 0.01 cm^{-1} for a porous fiber with diameter 380 μm and 40% porosity [15]. A non-destructive directional coupler method, where a second fiber is translated along the length of the test fiber, is used to measure the transmission losses [15]. Also during the characterization of the microstructured TOPAS THz fiber (fiber SMA with 28% porosity [6]) Nielsen et al. has observed THz microporous guidance at 0.2 THz [6]. No loss value has been reported for this fiber.

In this paper, to the best of our knowledge, we demonstrate the first fabrication of highly porous THz fibers with symmetrical and asymmetrical sub-wavelength air-holes and experimental characterization of their effective refractive indices (n_{eff}). The fabrication of these porous fibers can not be formed by stacking or drilling methods. The experimental results agree with the predicted effective refractive index values, which validates both the low dispersion characteristics of the porous fibers compared to their microwire counterparts and the birefringence characteristics for asymmetrical porous fiber.

2. Fiber design and fabrication

The polymer material used for the fabrication of porous fibers and microwire is Polymethyl methacrylate (PMMA), whose optical properties in the THz region are reported in Ref. [4]. As a reference, at 0.5 THz, the absorption coefficient and refractive index of the PMMA are 4.2 cm^{-1} and 1.65, respectively. The fibers are fabricated in a two-step process. First the preforms with the macroscopic structure are manufactured using the extrusion technique, which has been demonstrated to be not only viable for soft glasses [17] but also for polymers [18]. The preforms are extruded by heating up a bulk polymer billet to a temperature where the material gets soft (170-180 °C). Then the soft material is forced through an extrusion die using a ram extruder at a fixed speed. The die exit geometry determines the preform cross-section. In the next step, the preform of 10-15 mm diameter and 180 mm length is drawn down to bands of more than 10 meters of fibers with outer diameters of a few hundreds of microns using a fiber drawing tower.

The critical step in the porous fiber fabrication is the die design. As stated in Refs. [1, 10] the loss and dispersion of a porous fiber depends on the porosity of the fiber (fraction of the air-holes to the total core area) and the size (but not the shape) of the air-holes. We start the die design with an hexagonal array of circular air-holes, which is one of the most studied and

#111989 - $15.00 USD Received 1 Jun 2009; revised 24 Jul 2009; accepted 24 Jul 2009; published 29 Jul 2009

common arrangement of the air-holes in microstructured optical fibers. The cross-section of the die exit with hexagonal array of circular air-holes is shown in Fig. 1(a). The porosity achieved is limited to 47% due to extrusion die machining constraints, such as minimum wall thickness of 0.6 mm between the holes. In the fiber, the porosity will be even lower than the value given by the die exit due to thickening of the nodes between the air-holes [18]. Recent advances in the fiber preform extrusion and die design of microstructured fibers [17] have allowed us to fabricate fibers with non-circular and sub-wavelength size air-holes. This results in thiner layer of material between non-circular air-holes in comparision to the circular air-holes, which increases the achievable porosity for the fibers. This increase in porosity using the new die design opens up a new opportunities in THz porous fiber fabrication.

In this paper we consider two types of porous fibers: porous fiber with symmetrical and asymmetrical sub-wavelength air-holes. The cross-sectiones of the designed die exit for a symmetrical (here after called spider-web), and an asymmetrical (here after called rectangular), porous fibers are shown in Figs. 1(b) and 1(c), respectively. The cross-sectiones of the extruded preform of a spider-web and rectangular porous fibers are shown in Figs. 1(d) and 1(e), respectively.

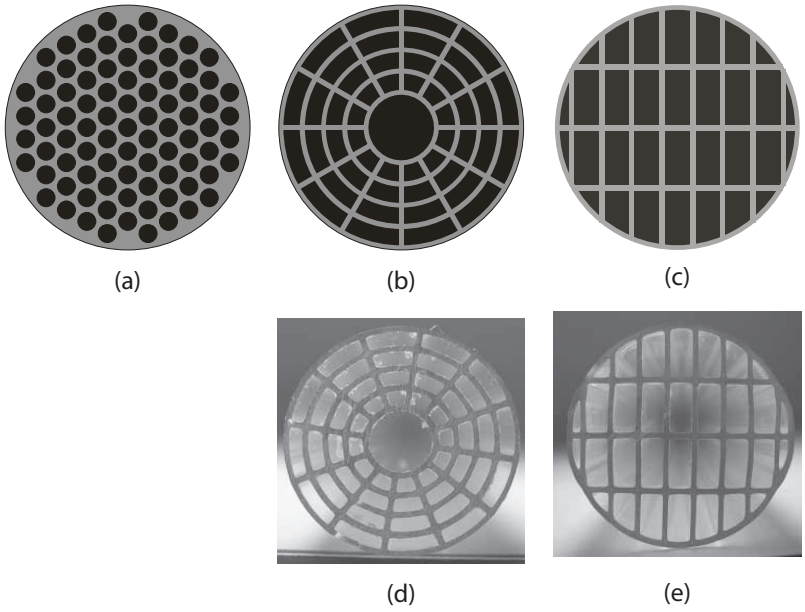

Fig. 1. The die design of the (a) hexagonal array of circular (b) spider-web and (c) rectangular air-hole porous fibers. The extruded preform of the (d) spider-web (12 mm diameter) and (e) rectangular (10 mm diameter) porous fibers. The cross-section of the (f) spider-web and (g) rectangular porous fibers.

Next the extruded preforms are drawn to porous fibers. A spider-web fiber preform of 120 mm diameter and 180 mm length was drawn down to two different outer diameters of 200-250 μm and 300-350 μm, where as rectangular fiber preform of 100 mm diameter and 180 mm length was drawn down to three different sets of outer diameters (350-400, 450-500, and 550-600 μm). The porosity of the spider-web and rectangular porous fibers given by the die design are 67% and 71%, respectively. Using scanning electron microscope (SEM) images, the porosity of the fibers is measured to be 57% and 65%, respectively, which is smaller than the porosity given by the die design due to rounding in the corners and thickening of the struts.

#111989 - $15.00 USD Received 1 Jun 2009; revised 24 Jul 2009; accepted 24 Jul 2009; published 29 Jul 2009

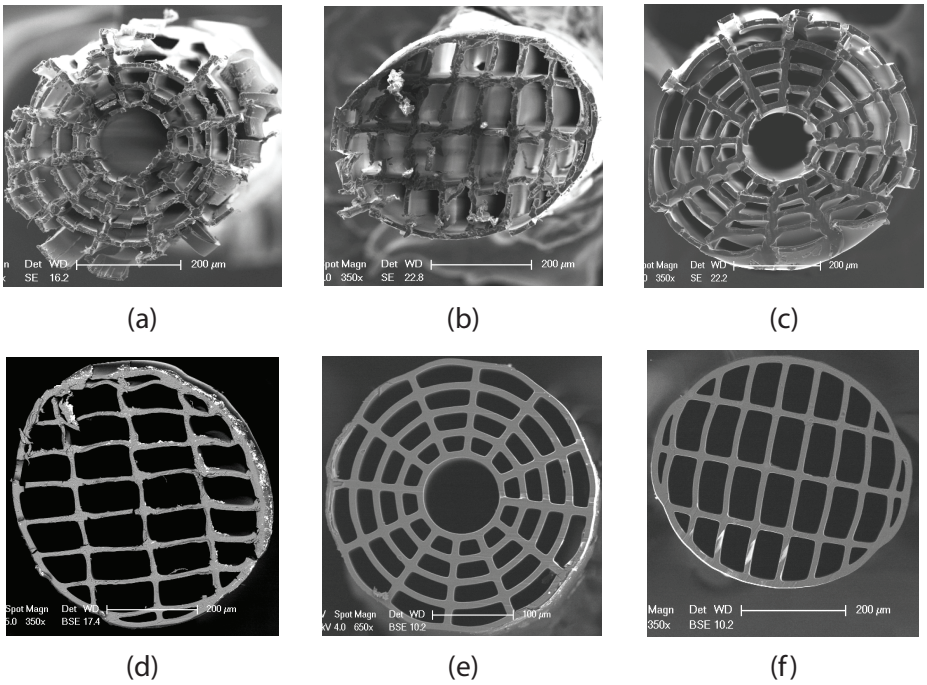

Fig. 2. Cleaved end-face of the (a) spider-web and (b) rectangular porous fibers using conventional blades. Cleaved end-face of the (c) spider-web and (d) rectangular porous fibers by heating up the blade and fiber before cleaving. Cleaved end face of the (e) spider-web and (f) rectangular air-hole porous fiber using focused ion beam milling.

The cleaving of these polymer porous fibers is non-trivial because they are easily squashed and deformed by using conventional cleaving blades, as shown in Figs. 2(a) and 2(b) for the spider-web and rectangular porous fibers, respectively. Heating up the cleaving blade and the fiber to 70-80°C as proposed by Law et al for microstructured polymer optical fibers [19], improves the cleaved end-face of the fibers. It is worth mentioning that the structure still gets deformed especially the outer ring, as shown in Figs. 2(c) and 2(d), because of high porosity and missing outer solid region as in optical microstructured fibers to date. Furthermore, we observe that as long as the cleaving force is in line with the struts of rectangular porous fiber, the achieved end-face of these fibers is better compared to the spider-web porous fibers.

The last method explored for cleaving the porous fibers is using focused ion beam (FIB) milling. The Gallium ions are accelerated to an energy of 30 keV (kiloelectronvolts), and then focused onto the sample. An ion beam current of 21 nA is used. The resulted cross-section of the FIB cleaved spider-web and rectangular porous fibers are shown in Figs. 2(e) and 2(f), respectively. The advantage of FIB milling to cleave porous fibers is that it provides smooth cuts across the entire fiber end-face. However, the amount of time required for cleaving a porous fiber with 400 μm diameter is about 17.5 hours.

To compare the properties of the porous fibers with a corresponding microwire, we also have used an extruded polymer optical fiber with 250 μm outer diameter [18] as a THz microwire. The THz properties of the billet used for microwire are same as that of the porous fiber.

#111989 - $15.00 USD Received 1 Jun 2009; revised 24 Jul 2009; accepted 24 Jul 2009; published 29 Jul 2009

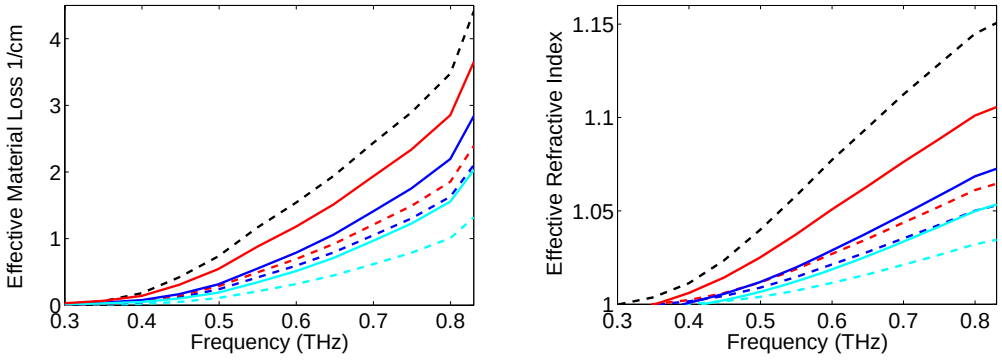

(a) (b)

Fig. 3. (a) Effective material loss and (b) effective refractive index of ideal (dashed lines) and real (solid lines) hexagonal array circular (black), spider-web (red) and rectangular (blue) porous fibers. The blue and cyan stand for the x- and y-polarizations of the fundamental mode of the rectangular porous fiber.

3. Porous fiber modeling and characterization

As discussed in the Section 2, due to rounding of the corners and thickening of the polymer struts during extrusion and fiber drawing, the cross-sections of the fabricated fibers [Figs. 2(e) and 2(f)] differ somewhat from the die exit cross-sections [Figs. 1(b) and 1(c)].

In order to observe the effect of the structure deformation on the THz properties of the fabricated porous fibers (α_{eff} and n_{eff}), the theoretical values of the effective material loss and effective refractive index of the *ideal* and *real* porous fibers are compared in Figs. 3(a) and 3(b). For the *ideal* porous fibers, the die exit cross-sections [Figs. 1(b) and 1(c)] are scaled down proportionally to a 350 μm outer diameter (the diameter of the fabricated porous fiber) and used for numerical modeling. While, for the *real* porous fibers, the SEM images of the cross-sections of the fabricated porous fibers [Figs. 2(e) and 2(f)] are used for numerical modeling. A Finite Element Modeling (FEM) technique instantiated in the commercial FEM package COMSOL 3.5 is used to calculate the theoretical values of the α_{eff} and n_{eff}. Different mesh densities are employed in different regions within the cross-section in order to achieve convergence for the calculated parameters. For comparison, the THz properties of a 300 μm diameter ideal circular shaped air-hole porous fiber with an hexagonal arrangement is also included. For this diameters, the effective material loss of the hexagonal array circular porous fiber at 0.3 THz is in the same order of magnitude compared with the spider-web porous fiber. Unsurprisingly the decrease in the porosity values of the fabricated fibers (due to rounding of the corners and thickening of the polymer struts) increases the value of the expected effective material loss and effective refractive index. Despite the increase, the characteristic values (α_{eff} and n_{eff}) for real spider-web and rectangular porous fibers are still lower than that of the ideal hexagonal array circular air-hole porous fiber.

The THz properties of the fabricated porous fibers are investigated by using terahertz time domain spectroscopy (THz-TDS). A mode-locked Ti:sapphire laser with a pulse width of less than 170 fs, central wavelength of 800 nm and a repetition rate of 76 MHz is used to drive the emitter, a photoconductive array of antennas [20], and the detector. The detector is a center-

#111989 - $15.00 USD Received 1 Jun 2009; revised 24 Jul 2009; accepted 24 Jul 2009; published 29 Jul 2009

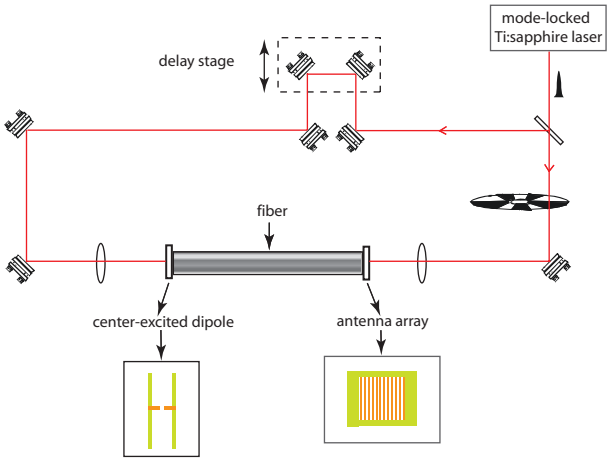

Fig. 4. Schematic of the terahertz time-domain spectroscopy setup. The emitter and detector are shown in the inset.

excited dipole between coplanar strip lines photoconductive switch with a 5 μm gap. The fiber tips are directly launched on the emitter and detector. The schematic of the THz-TDS setup and photoconductive antennas are shown in Fig. 4.

Assuming single mode propagation, the equation governing the input and output electric fields of the fiber can be written in the frequency domain as [21]:

$$E_{\text{out}}(\omega) = E_{\text{ref}}(\omega)\, T_1 T_2 C^2 \exp(-\alpha_{\text{eff}} L/2) \exp(-j\beta_{\text{eff}} L), \tag{1}$$

where, $E_{\text{out}}(\omega)$ and $E_{\text{ref}}(\omega)$ are the complex electric fields at angular frequency ω on the entrance and exit of the fiber, respectively; T_1 and T_2 are the total transmission coefficients that take into account the reflections at the entrance and exit faces, respectively; C is the coupling coefficient, the same for the entrance and exit faces; β_{eff} is the propagation constant of the fundamental mode; α_{eff} is the effective material loss that the propagating mode experiences; and L is the fiber length.

At least two different lengths of a fiber are required for calculating the THz properties (α_{eff} and β_{eff}) of the fiber. Applying Eq. (1) to two different lengths (L_1 and L_2), the transfer function determined from the ratio of $E_{\text{out1}}(\omega)$ and $E_{\text{out2}}(\omega)$ reads as:

$$\frac{E_{\text{out1}}(\omega)}{E_{\text{out2}}(\omega)} = \exp(-\alpha_{\text{eff}}(L_1 - L_2)/2) \exp(-j\beta_{\text{eff}}(L_1 - L_2)). \tag{2}$$

The C, T_1 and T_2 coefficients are canceled provided that the positions of the fiber and antenna does not change, e.g. this would occur during a cut back measurement. Then α_{eff} and β_{eff} of the fiber is obtained form the amplitude and the phase of the transfer function (Eq. (2)).

At this stage, it is not straight-forward to conduct a cut back measurement on porous fibers due to cleaving complexities discussed in Section 2. Therefore, three different lengths of each fiber are considered to determine the THz properties of spider-web and rectangular porous fibers. This introduces a large error in the loss measurement of the fibers, since the amplitude of the field guided by the fiber depends on the alignment of the fiber tip with the antenna (i.e. the coupling efficiency) and cleaved end-face of the fibers. However, the effective refractive index of the fibers, which depends on the phase of the transfer function and is independent from the C, T_1 and T_2 coefficients, can be determined.

#111989 - $15.00 USD Received 1 Jun 2009; revised 24 Jul 2009; accepted 24 Jul 2009; published 29 Jul 2009

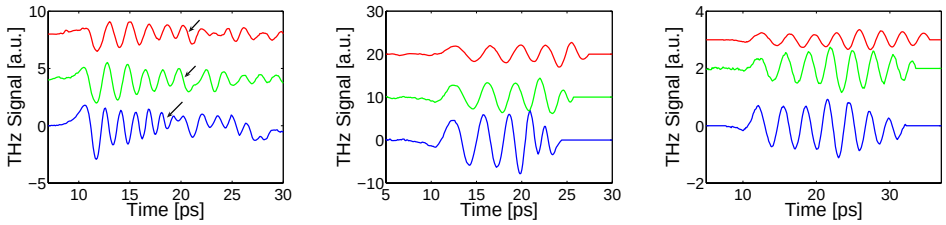

(a) (b) (c)

Fig. 5. (a)- The electric field of the terahertz pulse measured for (a) 200 μm and (b) 350 μm diameters of spider-web porous fiber and (c) 250 μm diameter of microwire. The top (red), middle (green) and bottom (blue) signals represents the measured terahertz pulse of long, medium and short length of fibers, respectively. The vertical offset has been introduced intentionally for clear display. The arrows in (a) indicate the cut-off point for each fiber length.

Figures 5(a), 5(b) and 5(c) show the electric fields of the terahertz pulse measured for three different lengths of a 200 μm and 350 μm diameter spider-web porous fibers and a 250 μm diameter microwire, respectively. The pulses are separated vertically for clear display. The red (top), green (middle) and blue (bottom) lines represent the pulses through the three different lengths, from the longest to shortest. The fiber lengths used for the 200 μm spider-web porous fiber are 24.4, 21.0 and 15.4 mm, the 350 μm spider-web porous fiber are 24.9, 20.4 and 16.0 mm and for the microwire are 25.0, 20.2 and 17.7 mm. Each pulse represent a single scan with a time constant of 1 s. Due to antenna structure there is reflection in the time domain signal at roughly 10 ps after the main pulse. In order to avoid artifacts caused by these reflection, the signals are cut-off at the zero crossing just before the reflection (shown with arrow points in Fig. 5(a)) and padded with zeros. The same number of peaks are considered for the three lengths of each fiber structure.

The effective refractive index for the fiber is determined by averaging the three individual effective refractive indices obtained from comparison of each pair of the three scans. Figure 6(a) shows the experimental results measured for the 200 μm and 350 μm diameter spider-web porous fibers and the 200 μm diameter microwire together with the theoretically calculated values of the real fiber structures (obtained from SEM image).

There are two major sources of errors that are considered: fiber length and data processing uncertainties as explained as follows. A $\pm$0.1 mm variation is considered for the length uncertainty. In order to remove the low-frequency $1/f$ noise two techniques have been used, which are base line removal and high pass filtering. The difference between these methods and the effect of variation of the cut-off frequency of the high pass filter are considered as the source of data processing uncertainty. The error bars shown in Fig. 6(a) represent the quadrature sum of standard deviations obtained from two sources of uncertainty described above. There is a good agreement between the theoretical and experimental calculated values of effective refractive indices. It is worth mentioning that the difference between the experimental and theoretical values at lower effective refractive index values is most likely due to the slight bending of the fibers.

Figure 6(a) indicates that the refractive index of porous fibers are a relatively flat function of frequency relative to that of the microwire. This corresponds to a slight drop in the group velocity of porous fiber compared to that of the microwire resulting in lower dispersion for

#111989 - $15.00 USD Received 1 Jun 2009; revised 24 Jul 2009; accepted 24 Jul 2009; published 29 Jul 2009

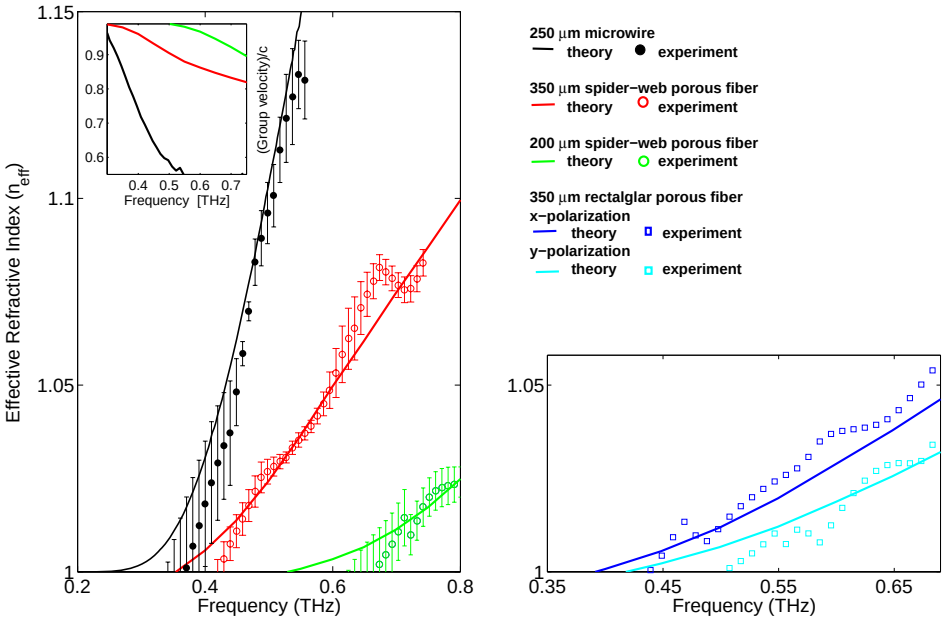

(a) (b)

Fig. 6. Efective refractive index of a 200 μm (green) and a 350 μm (red) diameters of spider-web porous fiber, a 250 μm diameter microwire (black) and a 350 μm diameter of rectangular porous fiber *x*-polarization (blue) and *y*-polarization (cyan) as a function of frequency. The solid lines represent the theoretical results based on the real fiber while the circles represent the measured experimental results.

THz porous fiber, as discussed in Ref. [10]. For further clarification the theoretical calculated normalized group velocity ($v_g = \partial\omega/\partial\beta_{\text{eff}}$) for the real 200 μm and 350 μm diameter spider-web porous fibers and the microwire is shown in the inset of the Fig. 6(a).

The experiment is repeated to define the THz properties of the *x*- and *y*-polarization of the fundamental mode of a 350 μm diameter rectangular porous fiber. The fiber is mounted on a rotational mount and the alignment of the tip of the fiber with the photoconductive antenna is monitored with a magnifier. The *x*- and *y*-polarization modes are acquired when the generated THz pulse on the antenna is parallel to the long and short sides of the rectangles, respectively. The fiber lengths considered for the experiment are 30.0, 34.1 and 38.2 mm.

Figure 6(b) shows the experimentally measured refractive indices of the *x*- and *y*-polarization modes for the 350 μm diameter rectangular porous fiber together with the theoretically calculated values of the real fiber structure. Experimentally, a 0.012 birefringence is achieved for 0.65 THz which is comparable to the expected theoretical results. As mentioned before for the lower effective refractive indices, the experimental data does not match well with the theory and this can be attributed to unwanted fiber bending. The slight oscillation in the measured n_{eff} values could be due to the different signal noise levels of the three lengths. It should be noted that the theoretical calculations based on the SEM image of the fabricated porous fibers confirm

#111989 - $15.00 USD Received 1 Jun 2009; revised 24 Jul 2009; accepted 24 Jul 2009; published 29 Jul 2009

that these fibers are in their single mode operating regime.

4. Conclusion and discussion

In conclusion, we successfully produced spider-web (symmetrical) and rectangular (asymmetrical) air-hole shaped porous fibers with high porosity of 57% and 65%, respectively. The porous polymer fibers are mechanically soft and therefore require non-trivial cleaving. Among the methods applied, the best cleaving quality is obtained when FIB milling is employed.

The calculated effective material loss and effective refractive index of the ideal and real spider-web and rectangular porous fibers show that an $\alpha_{\text{eff}} < 0.25$ cm^{-1} for $f < 0.8$ THz can be achieved. The good agreement between the measured and calculated n_{eff} indicated the low dispersion characteristics of these porous fibers compared to microwires. A birefringence of 0.012 at 0.65 THz was achieved for the rectangular porous fiber. This confirms that these fibers, with low loss and low dispersion that can be practically designed to maintain polarization of the field, are a promising polymer waveguide solution and a good substitute for free-space THz propagation. This also opens up new opportunities in THz biosensing, where the porous fibers can be used to sense ultra small sample sizes.

In order to measure the effective material loss of the fibers, it is required to implement either a cut-back method [6] or directional coupler method [15], where the coupling parameters are not required. With the applied approach in this paper, it is not straight forward to measure the loss values of the porous fiber since the coupling parameters are highly dependent on the reproducibility of the quality of cleaved end-face of the fibers and the relative position of the fiber tips in respect to the antenna.

A practical consideration is the annealing of polymer porous fibers. This will reduce the stress generated during fiber drawing resulting in straighter fiber for experiment. Subsequently the radiation losses due to the fiber curvature will be suppressed. An alternate approach is the fabrication of the fibers using a soft glass such as F2, which has lowest loss in THz regime among the soft glasses suitable for structured preform extrusion [22]. Moreover, the cleaving of the fiber will be much easier compared to porous polymer fibers. However, the effective material loss will be higher than that of the PMMA.

Acknowledgments

This research was supported under the Australian Research Council's (ARC) *Discovery Projects* funding scheme (project numbers DP0556112 and DP0880436), Australian Research Council Nanotechnology Network (ARCNN) Overseas Travel Fellowship, and Adelaide University Research Abroad Scholarship. The authors gratefully acknowledge Roger Moore for fiber drawing from Centre of Expertise in Photonics, Leonard Green for FIB milling from Adelaide Microscopy Centre, and Markus Wächter from Institut für Halbleitertechnik at RWTH Aachen University for assistance with THz hardware. Useful discussion with Brian W.-H. Ng, Withawat Withayachumnankul, and Christophe Fumeaux of The University of Adelaide is gratefully acknowledged. T. Monro acknowledges the support of an ARC Federation Fellowship.

#111989 - $15.00 USD Received 1 Jun 2009; revised 24 Jul 2009; accepted 24 Jul 2009; published 29 Jul 2009